JACC: CARDIOVASCULAR IMAGING VOL. 3, NO. 8, 2010

ISSN 1936-878X/$36.00
PUBLISHED BY ELSEVIER INC. DOI:10.1016/j.jcmg.2010.05.011

iREVIEWS

STATE-OF-THE-ART PAPER

Assessment of Subendocardial Structure and Function

Tony Stanton, MBChB, PhD,* Thomas H. Marwick, MBBS, PhD*†
Brisbane, Australia; and Cleveland, Ohio

The combination of high energy expenditure and the borderline adequacy of perfusion make the subendocardium uniquely vulnerable to injury. Selective subendocardial involvement is usually a marker of subclinical disease. Technical advances in new noninvasive imaging modalities, especially in spatial resolution, now permit qualitative and quantitative assessment of subendocardial structure, function, and perfusion. Many newer techniques have the potential to provide superior prognostic information to current standard assessment methods. This review describes the contemporary capabilities of multiple imaging modalities for assessment of the subendocardium, and seeks to guide the clinician regarding the information and technical deficiencies of each modality. (J Am Coll Cardiol Img 2010;3:867–75) © 2010 by the American College of Cardiology Foundation

Differences in function, loading, coronary perfusion, and pathology of the subendocardium make this a unique component of the myocardium. The importance of subendocardial function to overall cardiac mechanics has long been recognized (1). At a cellular level, myocytes are bound together in sheets, or laminae, typically 4 cells thick, which allow the heart to contract in longitudinal, radial, and circumferential planes (2). These vectors are different in the subendocardium and subepicardium, as the laminae are almost perpendicular to each other. Subendocardial contraction is greatest in the longitudinal plane, with both electrical and mechanical activation at this level propagating from apex to base. Conversely, subepicardial contraction generates circumferential shortening and left ventricular (LV) twist. The impairment of contraction in either layer is typically compensated by augmentation of the other (3). This compensatory mechanism allows preservation of overall LV ejection fraction in the face of abnormal diastolic function, but may be the harbinger of future systolic dysfunction if disease evolves to transmural involvement.

The subendocardium is vulnerable to change early in the course of disease due to several factors; it is the furthest layer from epicardial coronary flow, it undergoes extreme fluctuations in pressure and compression in both systole and diastole, and also appears prone to early structural microvascular architectural change such as fibrosis (4). Thus, the subendocardium is often the earliest myocardial layer affected in many disease processes. Advances in noninvasive imaging, and in particular improvements in spatial and temporal resolution, have allowed the investigation of disease processes within the subendocardium, identifying both perfusion and functional abnormalities. This has led to greater understanding of both

From the *University of Queensland, Brisbane, Australia; and the †Cleveland Clinic, Cleveland, Ohio. Supported by a Project grant (456139) from the National Health and Medical Research Council, Canberra, Australia.

Manuscript received November 23, 2009; revised manuscript received April 28, 2010, accepted May 4, 2010.

disease mechanisms and possible treatment strategies. This understanding may allow us to better understand the progression of disease from diastolic dysfunction to overt systolic heart failure. In nonischemic heart failure with normal ejection fraction (HFNEF), arterial stiffness and fibrosis cause subendocardial function to be reduced both at rest and on exercise (5), resulting in diastolic dysfunction. Coronary ischemia also initially brings about diastolic dysfunction due to impairment of subendocardial perfusion prior to the development of overt systolic dysfunction (6).

This review will mainly focus on the contribution of recent imaging advances to evaluation of the subendocardium. For most clinicians, echocardiography remains the initial and most easily accessible cardiac imaging modality. Although this technique provides good spatial and excellent temporal resolution, other techniques offer higher contrast resolution. The optimal method to investigate subendocardial function will vary according to the question posed (Table 1).

ABBREVIATIONS AND ACRONYMS

2DS = 2-dimensional speckle

CMR = cardiac magnetic resonance

CT = computed tomography

CTA = computed tomography angiography

CVIB = cyclic variation of backscatter

LGE = late Gadolinium-DTPA enhancement

LV = left ventricular

MCE = myocardial contrast echocardiography

MDCT = multidetector computed tomography

PET = positron emission tomography

SPECT = single-photon emission computed tomography

Tissue Characterization of the Subendocardium

Integrated backscatter. Myocardial integrated backscatter is a modality used to assess the reflection of ultrasound waves from cardiac tissue. It can be measured as calibrated backscatter, whereby the reflection is normalized to adjacent high (e.g., pericardial) or low density (e.g., LV cavity) myocardium. Subendocardial scar has increased calibrated backscatter. Additionally, integrated backscatter varies throughout the cardiac cycle and is normally increased in systole (cyclic variation integrated backscatter [CVIB]) due to changes in acoustic properties related to tissue compression and alignment of reflectors (Fig. 1). Transmural CVIB is decreased in ischemic myocardial segments (7).

Normal contraction is heterogeneous, with subendocardial contraction being markedly greater than subepicardial contraction (1). By placing a manual region of interest in either the subendocardial or subepicardial half of the LV wall offline, Colonna et al. (8) localized the influence of stress-induced (atrial pacing) ischemia on subendocardial and subepicardial layers in 25 patients with known coronary artery disease and 12 controls. During stress in myocardial segments supplied by nonstenosed coronary vessels, the investigators were able to show a transmural gradient of CVIB from subendocardium to subepicardium. However, there was blunting of the CVIB signal exclusively in the subendocardial region in segments supplied by stenosed vessels (≥50% angiographically evaluated by 2 observers), elegantly illustrating the ability of this technique to reliably quantify differences in function between the subendocardial and subepicardial layers. Although this approach is technically challenging (including requiring the availability of raw data) and is limited to the anteroseptal and inferolateral walls because of anisotropy, the measurement of CVIB is closely linked to strain.

Computed tomography. Multidetector computed tomography (MDCT) has undergone rapid advances in recent years, with improvements in spatial and temporal resolution. Although attention has been on the delineation of coronary anatomy, recent advances have allowed direct imaging of the subendocardium.

Iodinated contrast agents (iomeperol and gadodiamide) used in MDCT (contrast enhanced [CE]-MDCT) have similar kinetics to gadolinium-DTPA as used in CE cardiac magnetic resonance (CMR). Gerber et al. (9) demonstrated that gated 16-slice CE-MDCT was able to distinguish between infarcted and normal myocardium with similar efficacy as CE-CMR in patients with acute and chronic myocardial infarcts. Two patterns were typically seen, an early hypoenhancement pattern was seen shortly after contrast administration (demonstrating subendocardial microvascular obstruction), and late hyperenhancement (reflecting increased distribution volume of contrast within the myocardium with reduced flow). Other investigators have shown similar findings (10–12) in both animal and patient studies.

Although these data are encouraging, the radiation required for MDCT remains a disadvantage compared with other imaging techniques. Table 2 documents the average effective radiation doses incurred as background and by various imaging modalities (13). An imaging procedure imparting 10 mSV is estimated to increase the lifetime risk of dying of a malignancy by 0.05% although factors such as patient age, race, and sex will also modify risk considerably (14).

The use of potentially nephrotoxic contrast agents is also of concern. Given these reservations, it may be reasonable to suggest that myocardial characterization using MDCT should only be un-

dertaken when noninvasive coronary imaging using MDCT is already planned.

CMR. The high spatial resolution of CMR makes it an ideal technique for subendocardial imaging. Additionally, it requires neither radiation nor imaging "windows." Faster techniques have also improved the ability of the technique to satisfy clinical demand.

Late gadolinium-DTPA enhancement (LGE) is the main technique applied to visualize the subendocardium with a spatial resolution that is unattainable with standard methods (Fig. 2). Gadolinium accumulates in the interstitial space of areas of abnormal myocardium due to its delayed washout kinetics. Uptake produces a bright signal because it shortens the T1 time of tissues. This development has led to the application of LGE in a variety of conditions. There is a risk of nephrogenic systemic fibrosis following gadolinium administration in those with renal impairment (typically classified as creatinine clearance <30 mg/dl). Subendocardial gadolinium uptake was shown by Kim et al. (15) to closely correlate with histopathological tissue damage after myocardial infarction (16). Further studies have shown tissue viability to be predicted by the transmurality of LGE after myocardial infarction. Typically, the subendocardial distribution of LGE in coronary artery disease allows differentiation from myocarditis, which more commonly causes a mid-wall LGE pattern (17). LGE has also allowed the identification of subendocardial dysfunction in other conditions apart from coronary artery disease. Hosch et al. (18) demonstrated that LGE in amyloidosis was predominately subendocardial and correlated well with histopathological examination. Maceira et al. (19) have subsequently shown that the intramyocardial T1 difference between the subendocardium and subepicardium was a powerful predictor of prognosis in this patient group. Abnormal subendocardial LGE has also been shown in Churg-Strauss syndrome, Loeffler's endocarditis, and systemic sclerosis (20).

Myocardial strain and torsion can also be undertaken using CMR tagging or analogous techniques to evaluate 3 planes of cardiac motion. Ventricular twist (torsion) is often affected early in subclinical disease. As torsion is based on the mechanical advantage of epicardial fibers, this is an indirect measure of function in the subendocardium relative to the subepicardium. Subsequent abnormalities in torsion have been identified in patients with hypertrophic cardiomyopathy (21) and aortic stenosis (22) using CMR tagging. Restoration of subendocardial perfusion and contraction after cardiac surgery has been shown to ameliorate this (23).

Table 1. Strengths and Weaknesses of Different Imaging Modalities

Modality	Repeatable	Accessible	Regional Function	Reproducible	Patient Friendly
Echocardiography	++	++	+	+	++
Nuclear	+	+	+/−	+	+
MDCT	+	+	+	+	+
CMR	+	+/−	++	++	+

+/− = fair; + = good; ++ = excellent.
CMR = cardiac magnetic resonance; MDCT = multidetector computed tomography.

Assessment of Subendocardial Function

Deformation analysis. Long-axis function, representing subendocardial function, has long been estimated using mitral annular planar systolic excursion (MAPSE), although this displacement measure ignores the time course of contraction, which is a vital aspect of function (24). Advances in echocardiography have allowed both the rate of

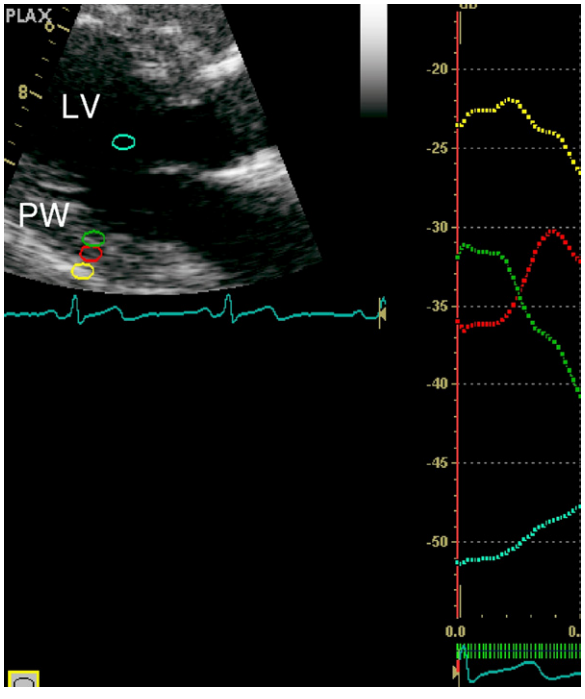

Figure 1. Integrated Backscatter of the PW During Systole, Consistent With Subendocardial Scar and Ischemia

The pericardium **(yellow)** is most reflective (i.e., least negative) and the cavity **(turquoise)** is least reflective (most negative). The subendocardium **(green)** is slightly more reflective than the epicardium **(red)**, but the epicardium thickens, and fiber thickening causes increased reflectivity. LV = left ventricle; PW = posterior wall.

Table 2. Radiation Dosage From Imaging Modalities

Imaging Modality	Effective Does (mSv)
1-year background radiation	2.4
Chest X-ray	0.1
CT	
Calcium score	2
Prospectively triggered CTCA	3
SPECT	
^{201}Tl	17
^{99c}Tm	10
PET	13
Invasive coronary angiography	7

Adapted from Einstein et al. (13) and Gerber et al. (14).
CT = computed tomography; CTCA = computed tomography coronary angiography; PET = positron emission tomography; SPECT = single-photon emission computed tomography; Tl = thallium; Tm = technetium.

deformation (strain rate) and the magnitude of deformation (strain) to be quantified, either based on longitudinal deformation (as this reflects the function of subendocardial fibers) or transmural distributions of deformation. These measurements were originally undertaken using tissue Doppler imaging, which has the technical limitations of angle dependence, signal noise, and measurement variability (25). The newer technique of 2-dimensional speckle (2DS) tracking employs frame-by-frame tracking of individual speckles throughout the cardiac cycle, and is able to quantify contraction in each of the longitudinal, radial, and circumferential planes. As the subendocardium is often affected first in disease processes, the early detection of impairment of subendocardial function using these sensitive techniques may allow earlier therapeutic intervention.

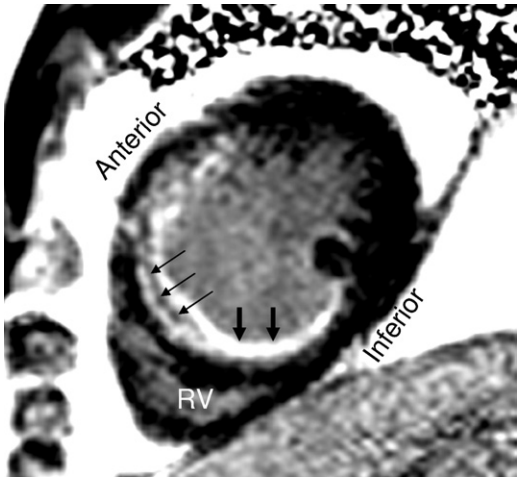

Figure 2. CMR Showing Extensive LGE in the Septum in a 49-Year-Old Man Presenting With an Acute Anterior Myocardial Infarction

The dark area in the anteroseptal region **(thin arrows)** signifies microvascular obstruction. The **thick arrows** indicate the late gadolinium enhancement (LGE). CMR = cardiac magnetic resonance; RV = right ventricle.

TISSUE DOPPLER IMAGING. Longitudinal strain and strain rate are able to accurately detect differences in function between 3 myocardial layers at rest and in a range of different hemodynamic loading conditions (26). Of particular note, strain rate was highly significantly correlated with invasive measurements of LV function (dP/dt).

In addition to the influence of the presence and extent of ischemia on strain rate (27), this technique is also able to reflect interstitial changes in the subendocardium such as those that occur in LV hypertrophy. The detrimental effects of LV hypertrophy and ischemia on subendocardial function are additive. The clinical importance of these changes in subendocardial function was underscored recently in a study of 223 individuals with normal LV function over 5 years of follow-up. Strain rate was the most powerful independent predictor of all-cause mortality in this group and provided incremental information to other standard clinical and echocardiographic variables (28).

In patients after aortic valve replacement, longitudinal deformation measures correlate with CE-CMR evidence of subendocardial LV fibrosis, and predict functional improvement better than ejection fraction or aortic valve area (29). Similarly, radial strain analysis of healthy controls and patients with hypertension and aortic stenosis, show that the latter group—particularly in those with the classical electrocardiographic "strain" pattern—show inversion of the normal sequence of myocardial relaxation with subendocardial preceding subepicardial relaxation (30).

2DS TRACKING. 2DS tracking is an automated, quantitative technique that allows measurement of myocardial function in all 3 planes of cardiac motion. Frame-by-frame tracking of grayscale images (typically at a frame rate 50 to 70 fps) allows measurement of deformation based on excursion between individual speckles throughout the cardiac cycle. 2DS is more feasible than tissue velocity imaging–derived strain indexes (25), and has been validated against sonomicrometry and CMR tagging (25,31). As with tissue velocity imaging strain, 2DS can provide further insight into subclinical disease; abnormal longitudinal regional speckle strain in hypertensive patients is thought to detect subclinical LV function abnormalities that are not identified by ejection frac-

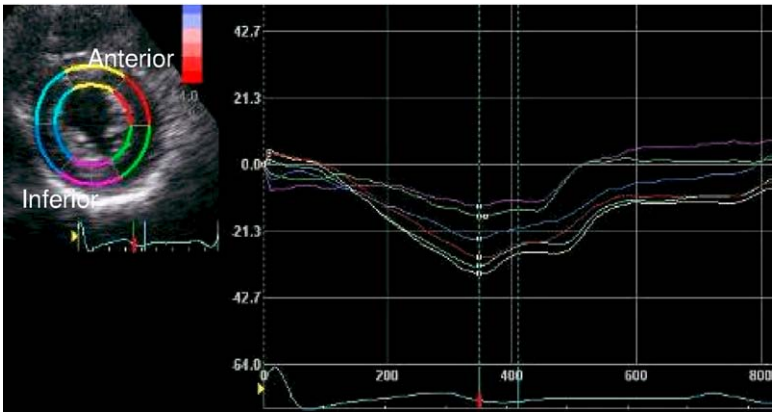

Figure 3. Measurement of Circumferential Strain in a Patient With Nontransmural Inferoposterior Infarction

Strains in this territory (corresponding to the **green and purple lines**) are reduced to about 50% of those in remote regions.

tion alone (32). Patterns of impairment of circumferential or longitudinal deformation may reflect transmural and subendocardial involvement, respectively (Fig. 3). These patterns have been used in the distinction of restrictive cardiomyopathy from constrictive pericarditis (33), as well as the identification of subendocardial scar (34,35). Indeed, any disease process preferentially affecting the subendocardium results in impairment of longitudinal function with preservation of circumferential function and torsion. The reverse pattern is seen in subepicardial disease. Finally, global longitudinal strain, a marker of subendocardial function, was shown to be incremental to standard baseline demographics and superior to ejection fraction and wall motion scoring index for the prediction of all-cause mortality in 546 consecutive patients attending echocardiographic assessment of LV function (36). A global longitudinal speckle tracking strain value of −12% is not only analogous to an LV ejection fraction <35%, but also has similar predictive power.

Assessment of Subendocardial Perfusion

CMR. CMR perfusion is usually carried out using adenosine stress. The usual sequence is imaging of the first pass of gadolinium through the myocardium during stress, followed by resting perfusion images and then late enhancement (37). The high spatial resolution of the technique allows the relative alterations in myocardial blood flow in the subendocardium and subepicardium, although the deconvolution of the input function for absolute flow measurement is more difficult. This technique may be particularly useful in disease states where there are microvascular perfusion abnormalities at the subendocardial level, such as syndrome X and hypertensive heart disease (38–40) (Fig. 4).

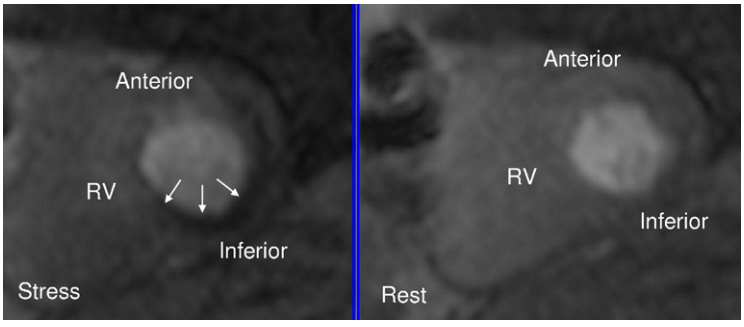

Figure 4. CMR Stress Perfusion

Stress perfusion image on the **left** shows inducible subendocardial defect **(arrows)** that is not matched in the resting image on the **right**. Coronary angiography revealed a tight circumflex coronary artery stenosis. Abbreviations as in Figure 2.

Table 3. Spatial Resolution of Imaging Modalities

Imaging Modality	Spatial Resolution (mm)
2D echocardiography	0.8
SPECT	3.8
PET	2.4
64-slice MDCT	0.4 × 0.4 × 0.4 (voxel size)
CMR (3-T)	0.7 × 0.7 × 0.7 (voxel size)

2D = 2-dimensional; other abbreviations as in Tables 1 and 2.

Table 4. Reproducibility of Subendocardial Imaging

Modality (Ref. #)	Intraobserver ICC	Interobserver ICC
Echocardiography		
TDI (28)	0.84	0.83
2DS (36)	0.92	0.92
MCE (49)	Not quoted	0.88
PET	Not quoted	Not quoted
MDCT (9)	0.81	0.88
CMR	0.93	0.84

2DS = 2-dimensional speckle tracking strain; ICC = intraclass correlation coefficient; MCE = myocardial contrast echocardiography; TDI = tissue Doppler imaging; other abbreviations as in Tables 1 and 2.

In hypertrophic cardiomyopathy (41), reduction of the vasodilator response, microvascular dysfunction, and subsequent ischemia are particularly prevalent in the subendocardium and are linked to the degree of hypertrophy. Abnormalities of the endocardium/epicardial perfusion ratio can be used to detect transplant arteriopathy in heart transplant recipients (42).

Signal noise and artifact remain problems with current perfusion CMR techniques. Contraindications relating to implanted metallic objects (especially pacemakers) mean that this technique is unlikely to have the versatility of the alternatives.

CT. Recent developments in CT technology have also allowed the investigation of subendocardial perfusion. Subendocardial systolic hypoperfusion, but normal subendocardial diastolic perfusion with 64-slice CE-MDCT corresponds to ischemic segments as identified myocardial perfusion scintigraphy. However, the greater systolic perfusion in the basal segments reduces the sensitivity of the test to recognize ischemia of the right coronary artery compared to the left anterior descending coronary artery territory (78% vs. 93%) (43). The combination of CT angiography (CTA) with perfusion using dual-source CT provides comparable diagnostic accuracy to single-photon emission computed tomography (SPECT) (44). However, whereas the radiation dose of both techniques was comparable (Table 2), the use of CTA plus CT perfusion required a larger bolus of iodated contrast than standard CTA.

Myocardial perfusion scintigraphy. The lower spatial resolution of positron emission tomography (PET) and SPECT has restricted their use for the assessment of subendocardial perfusion to patients with hypertrophied myocardium (Table 3). Nonetheless, subendocardial ischemia on exercise has been demonstrated with SPECT in patients with hypertrophic cardiomyopathy (asymmetric septal hypertrophy >2.0 cm) (45). Subendocardial and subepicardial coronary flow reserve has been calculated with PET, allowing calculation of transmural coronary flow reserve distribution (46). Impairment of subendocardial flow reserve has been documented in aortic stenosis patients with the highest gradients and LV mass (47). In general,

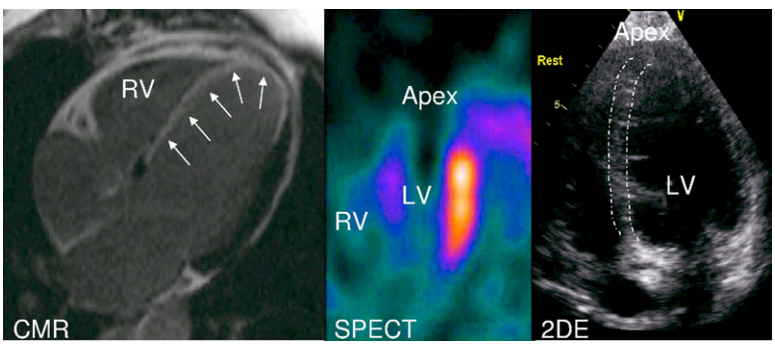

Figure 5. CMR, SPECT, and 2DE in a Middle-Aged Man After Acute Anteroseptal Myocardial Infarction

CMR shows extensive late gadolinium enhancement in the left anterior descending coronary artery (LAD) territory (**white arrows**), varying from subendocardial in the mid-septum to transmural in the apex. The degree of scar tissue exceeds the spatial resolution of SPECT (appears restricted to the apex), and the transmural extent cannot be recognized on standard resting echocardiography (septal thickness marked by **pecked lines**). 2DE = 2-dimensional echocardiography; SPECT = single-photon emission computed tomography; other abbreviations as in Figures 1 and 2.

however, the lower spatial resolution of SPECT and PET relative to the other imaging modalities, the radiation dosage required, and paucity of reproducibility data for subendocardial imaging continues to limit the use of these techniques (Table 4) (Fig. 5).

Myocardial contrast echocardiography (MCE). Subendocardial ischemia was visualized in humans using myocardial contrast echocardiography (MCE) 20 years ago (48), but is more difficult using intravenous injection. The development of real-time MCE has permitted the detection of subendocardial ischemia during dobutamine stress echocardiography (49), even when wall thickening is unaffected (Fig. 6). Although the lack of radiation exposure, convenience of access, and real-time nature of this technique are all attractive, the technical challenges of MCE and the lack of an approved microbubble for this purpose have contributed to the failure of MCE to achieve routine clinical use.

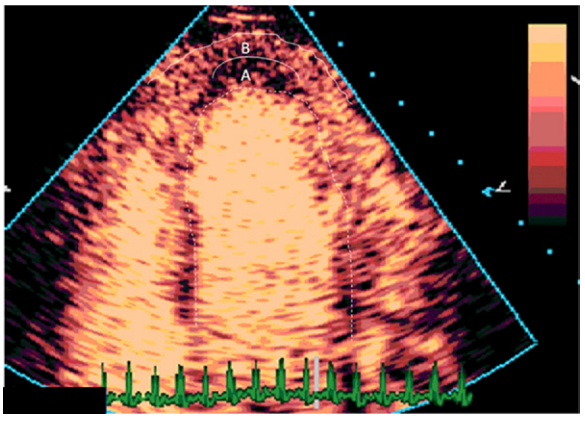

Figure 6. Identification of Subendocardial Malperfusion in the Apex Using MCE

The perfusion defect is in a subendocardial location **(A, dark area)**, surrounded by preserved subepicardial perfusion **(B, bright area)**. MCE = myocardial contrast echocardiography.

Conclusions

The subendocardium is unique in its susceptibility to disease processes. Its anatomical position, unique myocardial fiber orientation, and susceptibility to massive pressure alterations make it the harbinger of future overt cardiac dysfunction. Recent advances in both temporal and spatial image resolution have allowed assessment of both subendocardial function and perfusion. The ideal imaging technique should combine both of these elements without the need for radiation. Subendocardial imaging provides unprecedented insights into the disease process, allows the clinician to detect subclinical dysfunction, and introduces the possibility of new treatments specifically targeting the subendocardium (50).

Acknowledgments

The authors gratefully acknowledge the help of Dr. Alex Payne, Dr. Colin Berry, and Dr. Niko Tzemos for their help in acquiring the images used in Figures 2 and 4.

Reprint requests and correspondence: Dr. Thomas H. Marwick, Cardiovascular Imaging J1-5, Heart and Vascular Institute, Cleveland Clinic, 9500 Euclid Avenue, Cleveland, Ohio 44195. *E-mail: marwict@ccf.org.*

REFERENCES

1. Sabbah HN, Marzilli M, Stein PD. The relative role of subendocardium and subepicardium in left ventricular mechanics. Am J Physiol 1981;240: H920–6.
2. LeGrice IJ, Takayama Y, Covell JW. Transverse shear along myocardial cleavage planes provides a mechanism for normal systolic wall thickening. Circ Res 1995;77:182–93.
3. Sengupta PP, Narula J. Reclassifying heart failure: predominantly subendocardial, subepicardial, and transmural. Heart Fail Clin 2008;4:379–82.
4. Schwartzkopff B, Motz W, Frenzel H, Vogt M, Knauer S, Strauer BE. Structural and functional alterations of the intramyocardial coronary arterioles in patients with arterial hypertension. Circulation 1993;88:993–1003.
5. Tan YT, Wenzelburger F, Lee E, et al. The pathophysiology of heart failure with normal ejection fraction: exercise echocardiography reveals complex abnormalities of both systolic and diastolic ventricular function involving torsion, untwist, and longitudinal motion. J Am Coll Cardiol 2009;54:36–46.
6. Vinereanu D, Nicolaides E, Tweddel AC, Fraser AG. "Pure" diastolic dysfunction is associated with long-axis systolic dysfunction. Implications for the diagnosis and classification of heart failure. Eur J Heart Fail 2005;7: 820–8.
7. Picano E, Faletra F, Marini C, et al. Increased echodensity of transiently asynergic myocardium in humans: a novel echocardiographic sign of myocardial ischemia. J Am Coll Cardiol 1993;21:199–207.
8. Colonna P, Montisci R, Galiuto L, Meloni L, Iliceto S. Effects of acute myocardial ischemia on intramyocardial contraction heterogeneity: a study performed with ultrasound integrated backscatter during transesophageal atrial pacing. Circulation 1999;100:1770–6.
9. Gerber BL, Belge B, Legros GJ, et al. Characterization of acute and chronic myocardial infarcts by multidetector computed tomography: comparison with contrast-enhanced magnetic resonance. Circulation 2006;113:823–33.
10. Mahnken AH, Koos R, Katoh M, et al. Assessment of myocardial viability in reperfused acute myocardial infarction using 16-slice computed tomography in comparison to magnetic resonance imaging. J Am Coll Cardiol 2005;45:2042–7.

JACC: CARDIOVASCULAR IMAGING, VOL. 3, NO. 8, 2010
AUGUST 2010:867–75

11. Baks T, Cademartiri F, Moelker AD, et al. Multislice computed tomography and magnetic resonance imaging for the assessment of reperfused acute myocardial infarction. J Am Coll Cardiol 2006;48:144–52.
12. Lardo AC, Cordeiro MA, Silva C, et al. Contrast-enhanced multidetector computed tomography viability imaging after myocardial infarction: characterization of myocyte death, microvascular obstruction, and chronic scar. Circulation 2006;113:394–404.
13. Einstein AJ, Moser KW, Thompson RC, Cerqueira MD, Henzlova MJ. Radiation dose to patients from cardiac diagnostic imaging. Circulation 2007;116:1290–305.
14. Gerber TC, Carr JJ, Arai AE, et al. Ionizing radiation in cardiac imaging: a science advisory from the American Heart Association Committee on Cardiac Imaging of the Council on Clinical Cardiology and Committee on Cardiovascular Imaging and Intervention of the Council on Cardiovascular Radiology and Intervention. Circulation 2009;119:1056–65.
15. Kim RJ, Fieno DS, Parrish TB, et al. Relationship of CMR delayed contrast enhancement to irreversible injury, infarct age, and contractile function. Circulation 1999;100:1992–2002.
16. Selvanayagam JB, Porto I, Channon K, et al. Troponin elevation after percutaneous coronary intervention directly represents the extent of irreversible myocardial injury: insights from cardiovascular magnetic resonance imaging. Circulation 2005;111:1027–32.
17. Mahrholdt H, Wagner A, Deluigi CC, et al. Presentation, patterns of myocardial damage, and clinical course of viral myocarditis. Circulation 2006;114:1581–90.
18. Hosch W, Kristen AV, Libicher M, et al. Late enhancement in cardiac amyloidosis: correlation of CMR enhancement pattern with histopathological findings. Amyloid 2008;15:196–204.
19. Maceira AM, Prasad SK, Hawkins PN, Roughton M, Pennell DJ. Cardiovascular magnetic resonance and prognosis in cardiac amyloidosis. J Cardiovasc Magn Reson 2008;10:54.
20. Silva C, Moon JC, Elkington AG, John AS, Mohiaddin RH, Pennell DJ. Myocardial late gadolinium enhancement in specific cardiomyopathies by cardiovascular magnetic resonance: a preliminary experience. J Cardiovasc Med (Hagerstown) 2007;8:1076–9.
21. Young AA, Kramer CM, Ferrari VA, Axel L, Reichek N. Three-dimensional left ventricular deformation in hypertrophic cardiomyopathy. Circulation 1994;90:854–67.
22. Sandstede JJ, Beer M, Hofmann S, et al. Changes in left and right ventricular cardiac function after valve replacement for aortic stenosis determined by cine MR imaging. J Magn Reson Imaging 2000;12:240–6.
23. Setser RM, Kasper JM, Lieber ML, Starling RC, McCarthy PM, White RD. Persistent abnormal left ventricular systolic torsion in dilated cardiomyopathy after partial left ventriculectomy. J Thorac Cardiovasc Surg 2003;126:48–55.
24. Henein MY, Priestley K, Davarashvili T, Buller N, Gibson DG. Early changes in left ventricular subendocardial function after successful coronary angioplasty. Br Heart J 1993;69:501–6.
25. Cho GY, Chan J, Leano R, Strudwick M, Marwick TH. Comparison of two-dimensional speckle and tissue velocity based strain and validation with harmonic phase magnetic resonance imaging. Am J Cardiol 2006;97:1661–6.
26. Hashimoto I, Li X, Hejmadi Bhat A, Jones M, Zetts AD, Sahn DJ. Myocardial strain rate is a superior method for evaluation of left ventricular subendocardial function compared with tissue Doppler imaging. J Am Coll Cardiol 2003;42:1574–83.
27. Bjork Ingul C, Rozis E, Slordahl SA, Marwick TH. Incremental value of strain rate imaging to wall motion analysis for prediction of outcome in patients undergoing dobutamine stress echocardiography. Circulation 2007;115:1252–9.
28. Stanton T, Ingul CB, Hare JL, Leano R, Marwick TH. Association of myocardial deformation with mortality independent of myocardial ischemia and left ventricular hypertrophy. J Am Coll Cardiol Img 2009;2:793–801.
29. Weidemann F, Herrmann S, Störk S, et al. Impact of myocardial fibrosis in patients with symptomatic severe aortic stenosis. Circulation 2009;120:577–84.
30. Hasegawa T, Nakatani S, Kanzaki H, Abe H, Kitakaze M. Heterogeneous onset of myocardial relaxation in subendocardial and subepicardial layers assessed with tissue strain imaging: comparison of normal and hypertrophied myocardium. J Am Coll Cardiol Img 2009;2:701–8.
31. Amundsen BH, Helle-Valle T, Edvardsen T, et al. Noninvasive myocardial strain measurement by speckle tracking echocardiography: validation against sonomicrometry and tagged magnetic resonance imaging. J Am Coll Cardiol 2006;47:789–93.
32. Narayanan A, Aurigemma GP, Chinali M, Hill JC, Meyer TE, Tighe DA. Cardiac mechanics in mild hypertensive heart disease: a speckle-strain imaging study. Circ Cardiovasc Imaging 2009;2:382–90.
33. Sengupta PP, Krishnamoorthy VK, Abhayaratna WP, et al. Disparate patterns of left ventricular mechanics differentiate constrictive pericarditis from restrictive cardiomyopathy. J Am Coll Cardiol Img 2008;1:29–38.
34. Becker M, Ocklenburg C, Altiok E, et al. Impact of infarct transmurality on layer-specific impairment of myocardial function: a myocardial deformation imaging study. Eur Heart J 2009;30:1467–76.
35. Sjøli B, Ørn S, Grenne B, Ihlen H, Edvardsen T, Brunvand H. Diagnostic capability and reproducibility of strain by Doppler and by speckle tracking in patients with acute myocardial infarction. J Am Coll Cardiol Img 2009;2:24–33.
36. Stanton T, Leano R, Marwick TH. Prediction of all-cause mortality from global longitudinal speckle strain: comparison with ejection fraction and wall motion scoring. Circ Cardiovasc Imaging 2009;2:356–64.
37. Costa MA, Shoemaker S, Futamatsu H, et al. Quantitative magnetic resonance perfusion imaging detects anatomic and physiologic coronary artery disease as measured by coronary angiography and fractional flow reserve. J Am Coll Cardiol 2007;50:514–22.
38. Panting JR, Gatehouse PD, Yang GZ, et al. Abnormal subendocardial perfusion in cardiac syndrome X detected by cardiovascular magnetic resonance imaging. N Engl J Med 2002;346:1948–53.
39. Pilz G, Klos M, Ali E, Hoefling B, Scheck R, Bernhardt P. Angiographic correlations of patients with small vessel disease diagnosed by adenosine-stress cardiac magnetic resonance imaging. J Cardiovasc Magn Reson 2008;10:8.
40. Kawecka-Jaszcz K, Czarnecka D, Olszanecka A, et al. Myocardial perfusion in hypertensive patients with normal coronary angiograms. J Hypertens 2008;26:1686–94.
41. Petersen SE, Jerosch-Herold M, Hudsmith LE, et al. Evidence for microvascular dysfunction in hypertrophic cardiomyopathy: new insights from multiparametric magnetic resonance imaging. Circulation 2007;115:2418–25.
42. Muehling OM, Wilke NM, Panse P, et al. Reduced myocardial perfusion reserve and transmural perfusion gradient in heart transplant arteriopathy assessed by magnetic resonance imaging. J Am Coll Cardiol 2003;42:1054–60.

43. Nagao M, Matsuoka H, Kawakami H, et al. Quantification of myocardial perfusion by contrast-enhanced 64-MDCT: characterization of ischemic myocardium. AJR Am J Roentgenol 2008;191:19–25.

44. Blankstein R, Shturman LD, Rogers IS, et al. Adenosine-induced stress myocardial perfusion imaging using dual-source cardiac computed tomography. J Am Coll Cardiol 2009;54:1072–84.

45. Kawasaki T, Akakabe Y, Yamano M, et al. Gated single-photon emission computed tomography detects subendocardial ischemia in hypertrophic cardiomyopathy. Circ J 2007;71:256–60.

46. Lorenzoni R, Gistri R, Cecchi F, et al. Coronary vasodilator reserve is impaired in patients with hypertrophic cardiomyopathy and left ventricular dysfunction. Am Heart J 1998;136:972–81.

47. Rajappan K, Rimoldi OE, Dutka DP, et al. Mechanisms of coronary microcirculatory dysfunction in patients with aortic stenosis and angiographically normal coronary arteries. Circulation 2002;105:470–6.

48. Lim YJ, Nanto S, Masuyama T, et al. Visualization of subendocardial myocardial ischemia with myocardial contrast echocardiography in humans. Circulation 1989;79:233–44.

49. Xie F, Dodla S, O'Leary E, Porter TR. Detection of subendocardial ischemia in the left anterior descending coronary artery territory with real-time myocardial contrast echocardiography during dobutamine stress echocardiography. J Am Coll Cardiol Img 2008;1:271–8.

50. Slezak J, Tribulova N, Okruhlicova L, et al. Hibernating myocardium: pathophysiology, diagnosis, and treatment. Can J Physiol Pharmacol 2009;87:252–65.

Key Words: subendocardium ■ noninvasive ■ imaging ■ function ■ perfusion.